Transmission characteristics of photonic crystal fiber gas cell used in frequency stabilized laser

Chongde Huang (黄崇德)[1,2], Dijun Chen (陈迪俊)[1*], Haiwen Cai (蔡海文)[1], Ronghui Qu (瞿荣辉)[1], and Weibiao Chen (陈卫标)[1]**

[1] *Key Laboratory of Space Laser Communication and Detection Technology, Shanghai Institute of Optics and Fine Mechanics, Chinese Academy of Sciences, Shanghai 201800, China*

[2] *University of Chinese Academy of Sciences, Beijing 100049, China*

[*] *Corresponding author: djchen@siom.ac.cn;* [**] *corresponding author: hwcai@siom.ac.cn*

Received March 3, 2014; accepted April 29, 2014; posted online July 18, 2014

We measure the transmission characteristics of hollow-core photonic crystal fiber (HC-PCF) gas cells with ferrule- and fusion-spliced configurations, and near- and far-field images of the HC-PCF are observed. Results show that the center of mass (COM) of the far-field image varies with the laser frequency and temperature, and the moving COM relates to the oscillatory transmission. Using a model of the spatial interference, we first demonstrate that mainly the modes with asymmetric phase distributions affect the COM position. The frequency stabilization performances of the lasers are compared. The fusion-spliced gas cell shows better performance than the ferrule-spliced one.

OCIS codes: 060.2270, 060.4005, 140.3425, 350.6090.

doi: 10.3788/COL201412.080602.

CO_2 is one of the most important greenhouse gases. Measurements show that the CO_2 density in the atmosphere is presently higher than that in the past 420000 years; hence, understanding the evolution of CO_2 in the global scale is important[1]. The integrated path differential absorption (IPDA) lidar possesses advantages, such as high precision and low bias for measuring CO_2 density in the atmosphere. A frequency stabilized laser with a reference gas cell is a key in IPDA lidar technology[2,3]. Because the laser frequency is locked at the weak CO_2 R18 absorption line near 1572.02 nm, a gas cell with long optical path is necessary[2−4]. Hollow-core photonic crystal fibers (HC-PCFs) have been used to produce compact and robust gas cells with long absorption length[5,6]. The HC-PCFs are recently commercially available[7]. To build an all-fiber gas cell, coupling the HC-PCF with a standard single mode fiber (SMF) or a multimode fiber (MMF) is necessary. However, the gas cell often exhibits an oscillatory background in its transmission spectrum, which is considered due to the effect of HC-PCF's surface modes[8−10]. Our results show that the far-field of the HC-PCF's output changes with laser frequency, and leads to fluctuation of the power coupled to the subsequent fiber. Variations in background transmission result in spurious signals for the frequency reference and degrade the frequency stability of the seed laser.

In this letter, we compare the transmission characteristics of ferrule- and fusion-spliced HC-PCF gas cells. We measure the far-field pattern and variations in center-of-mass (COM) with the laser frequency and temperature. By performing the method of sliding-window Fourier transform on the transmission spectrum[11,12], the contents of the HC-PCF are analyzed, and their effective refractive indexes are deduced. A semi-empirical model based on the spatial interference between the HC-PCF modes is proposed to analyze the far-field variations. Here we reveal that variations in COM are mainly attributed to the coupling of the fundamental mode with the non-axial symmetric phase distribution modes, such as the LP_{11} and LP_{31}-like modes. The frequency stabilization performance of the laser is presented, and the fusion-spliced structure yields better results than the ferrule-spliced one.

The HC-PCF (HC-1550-02, NKT Photonics, USA) is used to make a compact and robust CO_2-filled gas cell with long absorption length for the laser as the frequency reference[5,6]. The core diameter of this HC-PCF is 10 μm and its attenuation is about 30 dB/km[7]. Two configurations of gas cells are made in our work, as shown in Fig. 1. The length of HC-PCF is 10 m in the ferrule-spliced configuration and 15 m in the fusion-splice configuration respectively. The input ports are both fusion-splicing with standard SMFs. The losses of the input splices are about 2 dB and they are repeatable. Because the core of the HC-PCF is larger than the SMF's, we connect the MMF of 50 μm core diameter to the HC-PCF's output end to reduce the insertion loss. For the ferrule-spliced configuration, the HC-PCF is sealed into a FC/PC ceramic ferrule and connected to the MMF with ceramic ferrule by a sleeve. There is a gap of about 20 μm between the two fibers, which is used to evacuate or fill the gas. Afterward, the splice is sealed with epoxy to keep the CO_2 gas with the required pressure. On the other hand, for the fusion-spliced configuration, the MMF is fusion splicing to the HC-PCF after filling CO_2 in the HC-PCF at the required pressure. The insertion loss of the ferrule-spliced gas cell is 3.5 dB, and the fusion-spliced gas cell's is 2.8 dB.

Here the light from a distributed-feedback laser diode (DFB-LD) is injected through the gas cells and a photo detector (PD) is used to record the transmission power. The transmission spectrums of the two gas cells are obtained by scanning the frequency of this DFB-LD. Figure 2 shows the measured curves in which fluctuations are noticed obviously. The percentages of peak-to-peak fluctuation to the average are 11.9% and 8.4%. Figure 3

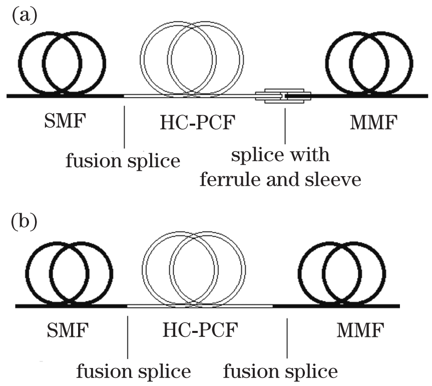

Fig. 1. Gas cells in the (a) ferrule-spliced and (b) fusion-spliced configurations.

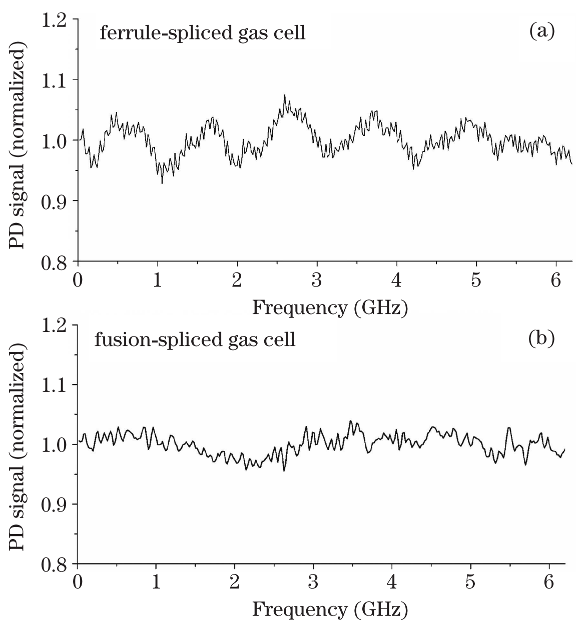

Fig. 2. The transmission spectra of (a) ferrule- and (b) fusion-spliced configurations.

shows the transmission spectra of the ferrule-spliced gas cell obtained under different temperatures; the spectra changes without obvious regularity when the temperature varies over about 0.6 °C. Obviously, the fluctuation of the transmission spectrum would lead to spurious signal for the frequency reference; especially the spectra would change with the temperature.

To understand the transmission characteristics, we observed the near-field pattern at the end of a 10-m-length HC-PCF using a 40× objective to focus the output beam to an InGaAs-based CCD camera, as shown in Fig. 4. The small spots surrounding the central peak are the surface mode, and the main spot comprises the fundamental mode and some higher-order modes (HOMs)[12,13]. The far-field pattern of HC-PCF was also measured by the CCD camera placed 10-mm away from the HC-PCF output end. The diameter of the main spot is about 4 mm. Variations in COM of the far-field profile with the laser frequency and temperature are observed, as shown in Fig. 5. The scanning range of laser frequency is over 6 GHz; the temperature changes over 2 °C. The two curves in Fig. 5 correspond to the x- and y- directions of the transverse cross-section. The change in COM with the laser frequency is a combination of two sinusoidal functions with different periods and amplitudes in the x-direction. The change in the y-direction has lower amplitude and with phase retard. Moreover, the change in COM with temperature is more complicated and irregular.

Such fluctuations in transmission are surely harmful to the function of HC-PCF gas cells[14]. Hence, understanding the mechanisms behind this phenomenon is necessary. It is known that not only the fundamental mode can exist in the HC-PCF[12−16]. The mode contents of the 10-m-length HC-PCF used in our work were analyzed by the sliding-window Fourier transform on the high-resolution

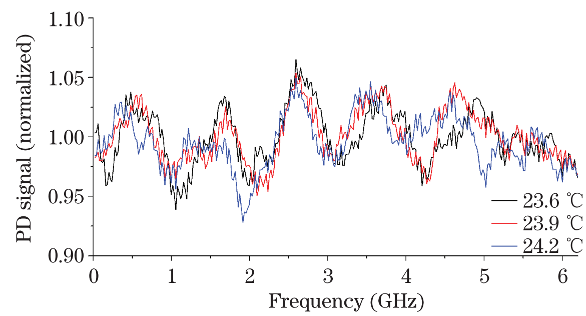

Fig. 3. (Color online) The transmission spectra of ferrule-spliced gas cell for different temperatures.

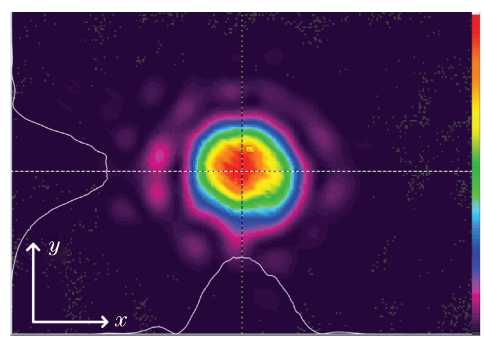

Fig. 4. (Color online) Near-field pattern of the HC-PCF output end.

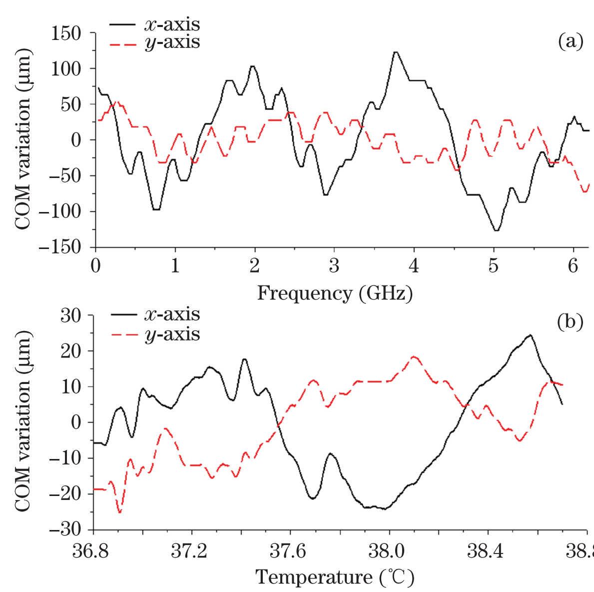

Fig. 5. (Color online) Changes in COM with (a) the laser frequency and (b) temperature.

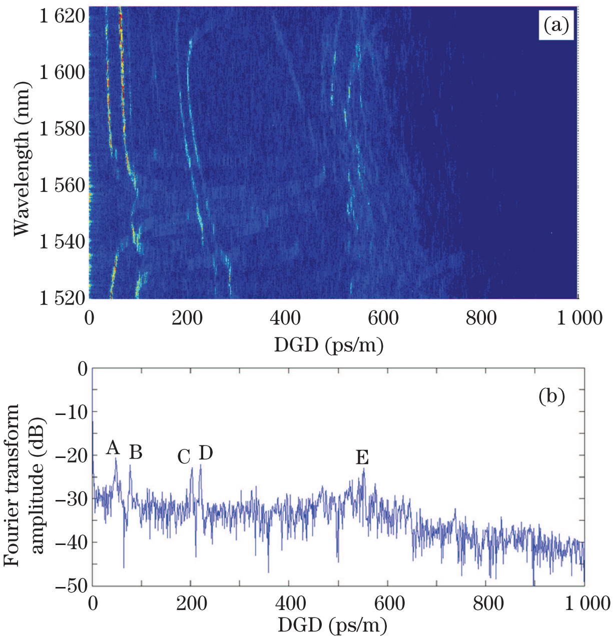

Fig. 6. (Color online) (a) Results of sliding-window Fourier transform on the transmission spectrum of the HC-PCF as a function of DGD and wavelength; (b) Fourier transform of the transmission spectrum at 1572 nm.

transmission spectrum[11,12]. We used a tunable external cavity laser as the frequency scanning source. The wavelength of the source was scanning from 1520 to 1620 nm and the step size was 2 pm. The light was injected into the HC-PCF and the transmission spectrum was recorded by the PD. When analyzing the data, a narrow window of about 2 nm was taken and swept across the full spectrum. The Fourier transforms are applied on the subset of the spectrums over these windows and stacked together to form an image showing the Fourier amplitude as the function of wavelength and differential group delay (DGD), as shown in Fig. 6(a). The DGD has been normalized to the HC-PCF length in ps/m. Figure 6(b) is a line out from Fig. 6(a) at the wavelength of 1572 nm and reveals that 5 HOMs exist at this wavelength, labeled as modes A, B, C, D, and E. Modes A to D have higher amplitudes than mode E. The effective refractive index of the modes can be calculated as

$$n_{\text{eff}} = n_0 - c\tau/L, \tag{1}$$

where n_0=1 is the refractive index of the fundamental mode, c is the speed of light, L is the HC-PCF length, and τ is the group delay in the length L. The effective refractive indexes of these modes calculated with the measured τ at 1572 nm are: n_{A}=0.9856, n_{B}=0.9766, n_{C}=0.9391, n_{D}=0.9310, n_{E}=0.8325.

The ideal HC-PCF has modes similar to those of the step-index fiber modes. The measured changes in COM are analyzed with a model based on the spatial interference of the HOMs[15]. Referring to the analyses in Refs. [15−17], modes A to D correspond to the LP_{11}-, LP_{21}-, LP_{02}-, and LP_{31}-like modes. Figure 7 shows the calculated profiles of these modes which have a π-shifted phase difference between the adjacent lobes[18]. When the laser frequency or the temperature changes, the relative phases between the modes change and result in variations in COM because of the spatial interference. The far-field profile is calculated by Fresnel diffraction theory upon considering all of the modes.

Figure 8(a) illustrates the calculated variations in COM as a function of the frequency in the x-direction. The curve is composed of two quasi-sinusoids with different periods and amplitudes. The interferences between the fundamental mode and LP_{11}- and LP_{31}-like modes give the main contributions. Here, the modes possess asymmetric phase distributions to y-axis; as well, the LP_{21}-like mode possesses a symmetric phase distribution; the LP_{02}-like mode possesses cylindrical symmetry. The simulations based on the spatial interference model considerably agree with the experimental results in Fig. 5(a).

Variations in COM with temperature are analyzed using the same model. We inferred that the temperature changed the fiber length by thermal expansion, and also changed the effective index; therefore the relative phases of different HOMs at the output end facet changed, and resulted in COM's variations in the far-field pattern. Figure 8(b) shows the calculated variations in COM. The simulation shows a variation trend similar to the experimental curve shown in Fig. 5(b). The complicated and irregular details may be caused by the random temperature distribution along the fiber, and also the strain and vibration effects. The simulations reveal that the spatial interference model gives a convincing explanation of the experimental results.

It is reasonable to suppose that the changes in COM have contribution to the transmission fluctuation. Due to the effect of spatial filtering in the coupling to the MMF, the coupling efficiency between the HC-PCF and the MMF changes with the variations in COM and leads to the transmission fluctuation. In our work, the ferrule-spliced configuration has 20-μm gap between the HC-PCF and the MMF, while the fusion-spliced configuration is connected without the gap. Therefore, the spatial filtering effect of the ferrule-spliced configuration is more obvious than the fusion-spliced one. Comparing Figs. 2(a), 5(a), and 8(a), the transmission has a low-frequency variation whose period is about twice of the low-frequency variation in COM. It is inferred that the transmission gets maximum while the COM locates at

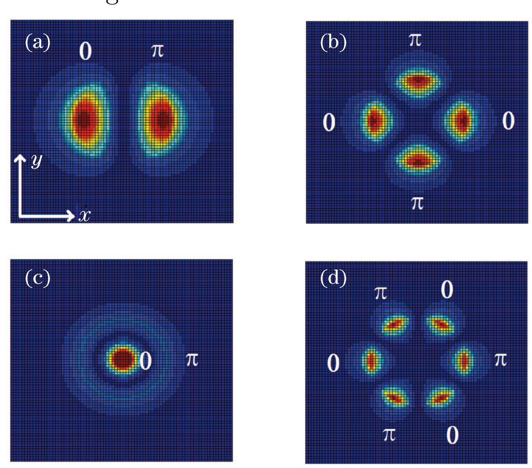

Fig. 7. (Color online) Calculated intensity and phase distributions of (a) LP_{11}-, (b) LP_{21}-, (c) LP_{02}-, and (d) LP_{31}-like modes.

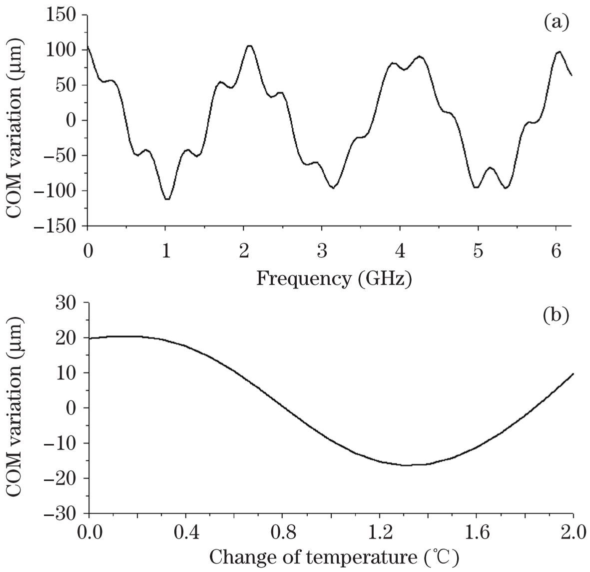

Fig. 8. The simulation results of changes in COM with (a) the laser frequency and (b) the temperature.

the center and gets minimum while the COM moves towards the sides. The transmission of the fusion-spliced gas cell has no such obvious fluctuation as shown in Fig. 2(b). Moreover, the transmission of the ferrule- and fusion-spliced gas cells both have the high-frequency and fluctuation. We suppose that is caused by the effects of surface modes instead of the core modes[9,14].

The laser frequency stabilization performances of the two configurations of gas cells are compared experimentally. The frequency of the DFB-LD is locked on the CO_2 Doppler-broadened R18 absorption line at 1572.02 nm by the frequency modulation spectroscopy technique, which is similar to the well-known PDH technique[3,19,20]. The laser is modulated by a phase modulator driven by a 130-MHz sinusoidal radio frequency (RF) signal at a modulation index of ~2.1. Subsequently the light is injected through the CO_2 gas cell which pressure is ~60 mbar. The output light is detected by a PD and its power is ~2 dBm. A demodulation circuit mixes the PD signal with the RF signal and produces an error signal to feedback to the DFB-LD by a servo circuit. Figure 9(a) shows the scheme of the frequency stabilization laser. The CO_2 Doppler-broaden line and error signal from the ferrule- and fusion-spliced gas cells are shown in Figs. 9(b) and (c). Although the length of these two gas cells are different, the absorption line's depth and linewidth of the two gas cells are close. Especially, by adjusting the tunable amplifier in the mixer circuit, the slope of the error signal is almost the same. The background fluctuation of the gas cells is the main reason which causes the frequency drift.

In the experiment the gas cells were placed in a foam enclosure and the temperature was stabilized within 0.6 °C. Figure 10(a) illustrates the frequency stabilization performance of the same DFB-LD using the ferrule- and fusion-spliced gas cells respectively. The data is the typical result under several times of tests measured by the Bristol 721 spectrum analyzer. The frequency drift of the fusion-spliced gas cell is subtracted by 30 MHz to give a clearer view. Figure 10(b) shows the Allan deviation versus the time. The frequency stabilization for the fusion-spliced gas cell reaches about 2.6×10^{-9} at 10 s and 1.2×10^{-9} at 1000 s, and that is about 1.1×10^{-8} at 10 s and 1.5×10^{-8} at 1000 s for the ferrule-spliced gas cell. The fusion-spliced gas cell shows better performance to stabilize the laser frequency. Although the ferrule-spliced gas cell is more convenient for gas filling, the fusion-spliced gas cell is the best choice for lasers requiring higher stabilization.

In conclusion, the transmission characteristics of the ferrule- and fusion-spliced configurations of HC-PCF gas

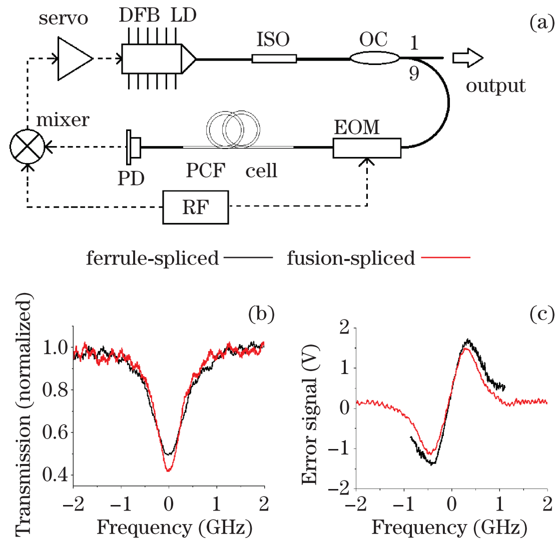

Fig. 9. (Color online) (a) The scheme of the frequency stabilization laser by frequency modulation spectroscopy technique, (b) the transmission spectrum of the fusion-spliced gas cell at the CO_2 R18 absorption line and (c) the corresponding error signal.

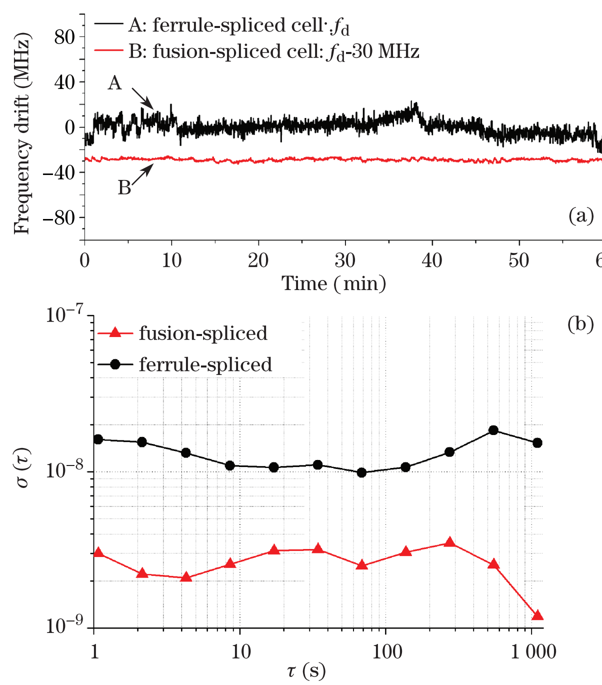

Fig. 10. (Color online) (a) The frequency stabilization performance of the ferrule- and fusion-spliced gas cell recorded for 1 hour and (b) the Allan deviation of frequency stabilization performance for the two gas cells respectively.

cells are analyzed experimentally. The transmission and output far-field COM of the HC-PCF are measured with scanning the laser frequency and varying the temperature. The mode contents of the HC-PCF are analyzed and simulations based on the spatial interference model give reasonable explanations of the experimental phenomena. The results show that the fusion-spliced gas cell shows lower transmission fluctuations and better frequency stabilization capability than the ferrule-spliced gas cell.

The author gratefully acknowledge Prof. Mao and Dr. Liu at Anhui Institute Optics and Fine Mechanics for providing the gas cells and helpful discussions. This work was supported in part by the National Natural Science Foundation of China (Nos. U0934001, 61108028, 61178031, and 61377062), the Science and Technology Commission of Shanghai Municipality (Nos. 11DZ1140202 and 13XD1425400), the Space Validation Project (No. MYHT-201104), and the Pudong New Area Science and Technology Development Fund, China (No. PKJ2012-D04).

References

1. J. R. Petit, J. Jouzel, D. Raynaud, N. I. Barkov, J. M. Barnola, I. Basile, M. Bender, J. Chappellaz, M. Davis, G. Delaygue, M. Delmotte, V. M. Kotlyakov, M. Legrand, V. Y. Lipenkov, C. Lorius, L. Pépin, C. Ritz, E. Saltzman, and M. Stievenard, Nature **399,** 429 (1999).
2. A. Fix, C. Budenbender, M. Wirth, M. Quatrevalet, A. Amediek, C. Kiemle, and G. Ehret, Proc. SPIE **8182,** 818206 (2011).
3. K. Numata, J. R. Chen, S. T. Wu, J. B. Abshire, and M. A. Krainak, Appl. Opt. **50,** 1047 (2011).
4. S. Yin and W. Wang, Chin. Opt. Lett. **4,** 360 (2006).
5. P. S. Light, F. Couny, and F. Benabid, Opt. Lett. **31,** 2538 (2006).
6. P. T. Marty, J. Morel, and T. Feurer, J. Lightw. Technol. **28,** 1236 (2010).
7. NKT Photonics' HC-1550-02 Datasheet, http://www.nktphotonics.com/files/files/HC-1550-02.pdf.
8. C. M. Smith, N. Venkataraman, M. T. Gallagher, D. Müller, J. A. West, N. F. Borrelli, D. C. Allan, and W. Koch, Nature **424,** 657 (2003).
9. C. Wang, N. V. Wheeler, C. Fourcade-Dutin, M. Grogan, T. D. Bradley, B. R. Washburn, F. Benavid, and K. L. Corwin, Appl. Opt. **52,** 5430 (2013).
10. C. I. Falk, J. Hald, J. C. Petersen, and J. K. Lyngsø, Appl. Opt. **49,** 3854 (2010).
11. J. M. Fini, J. W. Nicholson, R. S. Windeler, E. M. Monberg, L. Meng, B. Mangan, A. DeSantolo, and F. V. DiMarcello, Opt. Express **21,** 6233 (2013).
12. J. W. Nicholson, L. Meng, J. M. Fini, R. S. Windeler, A. DeSantolo, E. Monberg, F. DiMarcello, Y. Dulashko, M. Hassan, and R. Ortiz, Opt. Express **20,** 20494 (2012).
13. J. D. Shephard, P. J. Roberts, J. D. C. Jones, J. C. Knight, and D. P. Hand, J. Lightw. Technol. **24,** 3761 (2006).
14. K. Knabe, S. Wu, J. Lim, K. A. Tillman, P. S. Light, F. Couny, N. Wheeler, R. Thapa, A. M. Jones, J. W. Nicholson, B. R. Washburn, F. Benabid, and K. L. Corwun, Opt. Express **17,** 16017 (2009).
15. S. Wielandy, Opt. Express **15,** 15402 (2007).
16. F. Poletti, N. V. Wheeler, M. N. Petrovich, N. Baddela, E. N. Fokoua, J. R. Hayes, D. R. Gray, Z. Li, R. Slavík, and D. J. Richardson, Nature Photon. **7,** 279 (2013).
17. M. N. Petrovich, F. Poletti, and D. J. Richardson, in *Proceedings of 12th International Conference on Transparent Optical Networks* (*ICTON*) Tu.B2.3 (2010).
18. J. W. Nicholson, A. D. Yablon, J. M. Fini, and M. D. Mermelstrin, IEEE J. Sel. Top. Quant. Electron. **15,** 61 (2009).
19. Z. Bian, C. Huang, D. Chen, J. Peng, M. Gao, Z. Dong, J. Liu, H. Cai, R. Qu, and S. Gong, Chin. Opt. Lett. **10,** 019405 (2012).
20. M. Zhou, L. Huang, and X. Xu, Chin. Opt. Lett. **11,** 121402 (2013).